

IEEE TRANSACTIONS ON GEOSCIENCE AND REMOTE SENSING

A PUBLICATION OF THE IEEE GEOSCIENCE AND REMOTE SENSING SOCIETY



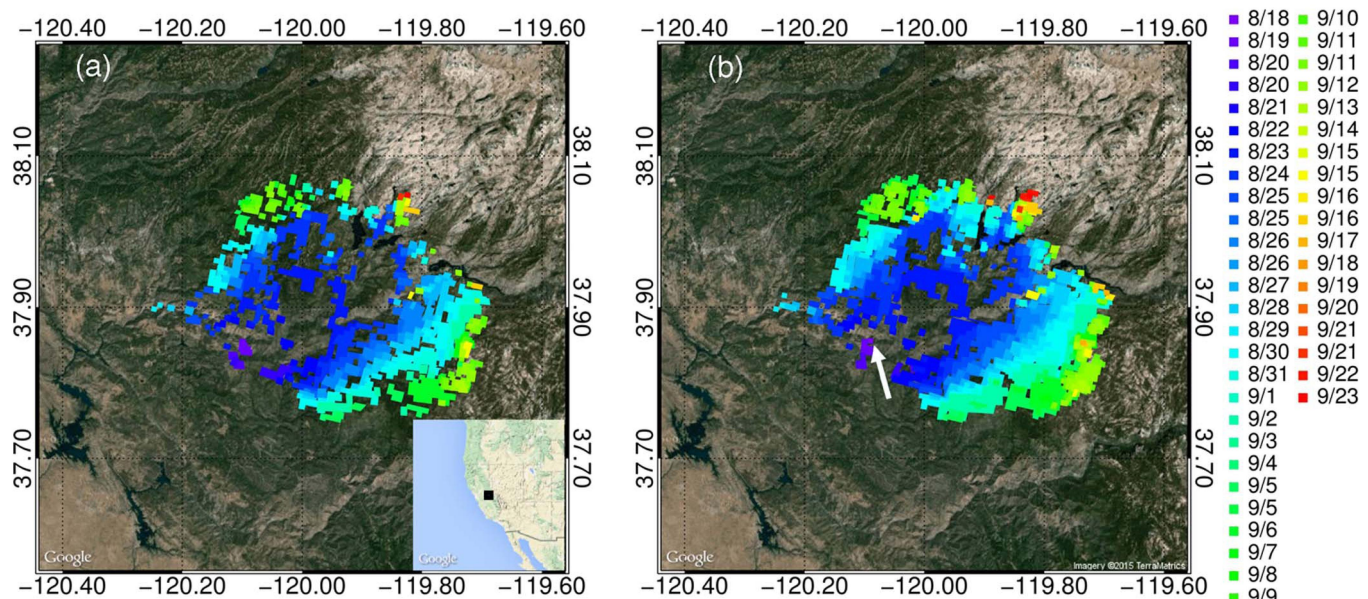
SEPTEMBER 2016

VOLUME 54

NUMBER 9

IGRSD2

(ISSN 0196-2892)



Progression of the 2013 Rim Fire from ignition to extinction, as revealed by the operational Active Fire Application Related Product (left) and the Firelight Detection Algorithm (right), both using the same input data from the VIIRS aboard the Suomi-NPP satellite.

IEEE TRANSACTIONS ON GEOSCIENCE AND REMOTE SENSING

A PUBLICATION OF THE IEEE GEOSCIENCE AND REMOTE SENSING SOCIETY



SEPTEMBER 2016

VOLUME 54

NUMBER 9

IGRSD2

(ISSN 0196-2892)

PAPERS

Atmosphere

- High-Spatial-Resolution Aerosol Optical Properties Retrieval Algorithm Using Chinese High-Resolution Earth Observation Satellite I *F. Bao, X. Gu, T. Cheng, Y. Wang, H. Guo, H. Chen, X. Wei, K. Xiang, and Y. Li* 5544

Vegetation and Land

- International Benchmarking of the Individual Tree Detection Methods for Modeling 3-D Canopy Structure for Silviculture and Forest Ecology Using Airborne Laser Scanning *Y. Wang, J. Hyppä, X. Liang, H. Kaartinen, X. Yu, E. Lindberg, J. Holmgren, Y. Qin, C. Mallet, A. Ferraz, H. Torabzadeh, F. Morsdorf, L. Zhu, J. Liu, and P. Alho* 5011
- CHP Toolkit: Case Study of LAIe Sensitivity to Discontinuity of Canopy Cover in Fruit Plantations *K. D. Fieber, I. J. Davenport, J. M. Ferryman, R. J. Gurney, V. M. Becerra, J. P. Walker, and J. M. Hacker* 5071
- Long-Time-Series Global Land Surface Satellite Leaf Area Index Product Derived From MODIS and AVHRR Surface Reflectance *Z. Xiao, S. Liang, J. Wang, Y. Xiang, X. Zhao, and J. Song* 5301

Subsurface and Geology

- Fundamental Analyses on Layered Media Reconstruction Using GPR and Full-Wave Inversion in Near-Field Conditions *A. De Coster, A. P. Tran, and S. Lambot* 5143
- Automatic Recognition of Long Period Events From Volcano Tectonic Earthquakes at Cotopaxi Volcano *R. A. Lara-Cueva, D. S. Benítez, E. V. Carrera, M. Ruiz, and J. L. Rojo-Álvarez* 5247
- A Probabilistic Model for Designing Multimodality Landmine Detection Systems to Improve Rates of Advance *J. M. Malof, K. D. Morton, Jr., L. M. Collins, and P. A. Torrione* 5258
- Seismic Simultaneous Source Separation via Patchwise Sparse Representation *Y. Zhou, J. Gao, W. Chen, and P. Frossard* 5271

Geodesy

- Use of a GPS-Derived Troposphere Model to Improve InSAR Deformation Estimates in the San Gabriel Valley, California *N. Houlié, G. J. Funning, and R. Bürgmann* 5365

Hyperspectral Data Processing

- Recursive Band Processing of Automatic Target Generation Process for Finding Unsupervised Targets in Hyperspectral Imagery *C.-I Chang and Y. Li* 5081

(Contents Continued on Page 5010)

| | |
|---|------|
| Tracking the Seasonal Dynamics of Boreal Forest Photosynthesis Using EO-1 Hyperion Reflectance: Sensitivity to Structural and Illumination Effects | 5105 |
| R. Hernández-Clemente, P. Kolari, A. Porcar-Castell, L. Korhonen, and M. Möttus | |
| Semiblind Hyperspectral Unmixing in the Presence of Spectral Library Mismatches | 5171 |
| X. Fu, W.-K. Ma, J. M. Bioucas-Dias, and T.-H. Chan | |
| Hyperspectral Image Classification Based on Spectral–Spatial One-Dimensional Manifold Embedding | 5319 |
| H. Luo, Y. Y. Tang, Y. Wang, J. Wang, L. Yang, C. Li, and T. Hu | |
| A Probabilistic Framework for Spectral–Spatial Classification of Hyperspectral Images | 5375 |
| J. Liu and W. Lu | |
| A New Methodology Based on Level Sets for Target Detection in Hyperspectral Images | 5385 |
| A. Alarcon-Ramirez, M. R. Rwebangira, M. F. Chouikha, and V. Manian | |
| Noise Removal From Hyperspectral Image With Joint Spectral–Spatial Distributed Sparse Representation | 5425 |
| J. Li, Q. Yuan, H. Shen, and L. Zhang | |
| Remote Sensing of 3-D Geometry and Surface Moisture of a Peat Production Area Using Hyperspectral Frame Cameras in Visible to Short-Wave Infrared Spectral Ranges Onboard a Small Unmanned Airborne Vehicle (UAV) | 5440 |
| E. Honkavaara, M. A. Eskelinen, I. Pöölönen, H. Saari, H. Ojanen, R. Mannila, C. Holmlund, T. Hakala, P. Litkey, T. Rosnell, N. Viljanen, and M. Pulkkanen | |
| Image Processing and Analysis | |
| Multiresolution Supervised Classification of Panchromatic and Multispectral Images by Markov Random Fields and Graph Cuts | 5054 |
| G. Moser, A. De Giorgi, and S. B. Serpico | |
| Spatiotemporal Subpixel Mapping of Time-Series Images | 5397 |
| Q. Wang, W. Shi, and P. M. Atkinson | |
| Weakly Supervised Learning Based on Coupled Convolutional Neural Networks for Aircraft Detection | 5553 |
| F. Zhang, B. Du, L. Zhang, and M. Xu | |
| Regression Wavelet Analysis for Lossless Coding of Remote-Sensing Data | 5616 |
| N. Anrani, J. Serra-Sagristà, V. Laparra, M. W. Marcellin, and J. Malo | |
| Inversion Methods | |
| Iterative ADMM for Inverse FE–BI Problem: A Potential Solution to Radio Tomography of Asteroids | 5226 |
| H. Su, F. Xu, S. Lu, and Y.-Q. Jin | |
| Microwave Radiometry | |
| Impact of the Soil Moisture Distribution in the Top Layer on the Accuracy Moisture Retrieval by Microwave Radiometer Data | 5239 |
| A. S. Yashchenko and P. P. Bobrov | |
| Experimental Study on Microwave Radiation From Deforming and Fracturing Rock Under Loading Outdoor | 5578 |
| S. Liu, Z. Xu, J. Wei, J. Huang, and L. Wu | |
| Radar Systems | |
| A Neural-Network-Based Beamformer for Phased Array Weather Radar | 5095 |
| T. Sallam, A. B. Abdel-Rahman, M. Alghoniemy, Z. Kawasaki, and T. Ushio | |
| Space-Time Adaptive Processing With Vertical Frequency Diverse Array for Range-Ambiguous Clutter Suppression | 5352 |
| J. Xu, G. Liao, and H. C. So | |
| Coastal Altimetry Products in the Strait of Gibraltar | 5455 |
| J. Gómez-Enri, P. Cipollini, M. Passaro, S. Vignudelli, B. Tejedor, and J. Coca | |
| NetRAD: Monostatic and Bistatic Sea Clutter Texture and Doppler Spectra Characterization at S-Band | 5533 |
| M. Ritchie, A. Stove, K. Woodbridge, and H. Griffiths | |
| Synthetic Aperture Radar | |
| Ground Moving Target Detection and Imaging Using a Virtual Multichannel Scheme in HRWS Mode | 5028 |
| L.-B. Wang, D.-W. Wang, J.-J. Li, J. Xu, C. Xie, and L. Wang | |
| Multiscale and Multidirectional Multilooking for SAR Image Enhancement | 5117 |
| A. Schmitt | |
| Long-CPI Multichannel SAR-Based Ground Moving Target Indication | 5159 |
| L. Xu, C. Gianelli, and J. Li | |
| Spaceborne/Stationary Bistatic SAR Imaging With TerraSAR-X as an Illuminator in Staring-Spotlight Mode | 5203 |
| H. Zhang, Y. Deng, R. Wang, N. Li, S. Zhao, F. Hong, L. Wu, and O. Loffeld | |
| Robust Two-Dimensional Phase Unwrapping for Multibaseline SAR Interferograms: A Two-Stage Programming Approach | 5217 |
| H. Yu and Y. Lan | |
| Nonlinear Model for InSAR Baseline Error | 5341 |
| G. Liu, R. F. Hanssen, H. Guo, H. Yue, and Z. Perski | |
| Polarimetric—Anisotropic Decomposition and Anisotropic Entropies of High-Resolution SAR Images | 5467 |
| F. Xu, Y. Li, and Y.-Q. Jin | |

| | | |
|---|--|------|
| Optimum Graph Cuts for Pruning Binary Partition Trees of Polarimetric SAR Images | <i>P. Salembier and S. Foucher</i> | 5493 |
| The Impacts of Building Orientation on Polarimetric Orientation Angle Estimation and Model-Based Decomposition for Multilook Polarimetric SAR Data in Urban Areas | <i>H. Li, Q. Li, G. Wu, J. Chen, and S. Liang</i> | 5520 |
| A New SAR-GMTI High-Accuracy Focusing and Relocation Method Using Instantaneous Interferometry | <i>S. Zhang, F. Zhou, G.-C. Sun, X.-G. Xia, M.-D. Xing, and Z. Bao</i> | 5564 |
| A Statistical Test of Phase Closure to Detect Influences on DInSAR Deformation Estimates Besides Displacements and Decorrelation Noise: Two Case Studies in High-Latitude Regions | <i>S. Zwieback, X. Liu, S. Antonova, B. Heim, A. Bartsch, J. Boike, and I. Hajnsek</i> | 5588 |
| A Depolarization Ratio Anomaly Detector to Identify Icebergs in Sea Ice Using Dual-Polarization SAR Images | <i>A. Marino, W. Dierking, and C. Wesche</i> | 5602 |
| Global Navigation Satellite System | | |
| First Ionospheric Radio-Occultation Measurements From GNSS Occultation Sounder on the Chinese Feng-Yun 3C Satellite | <i>T. Mao, L. Sun, G. Yang, X. Yue, T. Yu, C. Huang, Z. Zeng, Y. Wang, and J. Wang</i> | 5044 |
| GNSS Interferometric Radio Occultation | <i>M. Martin-Neira</i> | 5285 |
| Lidar Systems | | |
| A Three-Step Approach for TLS Point Cloud Classification | <i>Z. Li, L. Zhang, X. Tong, B. Du, Y. Wang, L. Zhang, Z. Zhang, H. Liu, J. Mei, X. Xing, and P. T. Mathiopoulos</i> | 5412 |
| Estimating the Solar Transmittance of Urban Trees Using Airborne LiDAR and Radiative Transfer Simulation | <i>H. Oshio and T. Asawa</i> | 5483 |
| UV/Visible/Infrared Imagers | | |
| Improving Nocturnal Fire Detection With the VIIRS Day–Night Band | <i>T. N. Polivka, J. Wang, L. T. Ellison, E. J. Hyer, and C. M. Ichoku</i> | 5503 |
| Satellite Systems | | |
| Tropical Mean Fluxes: A Tool for Calibration and Validation of CERES Radiometers | <i>G. L. Smith, S. Thomas, K. J. Priestley, and D. Walikainen</i> | 5135 |
| Reconstruction of GF-1 Soil Moisture Observation Based on Satellite and <i>In Situ</i> Sensor Collaboration Under Full Cloud Contamination | <i>X. Zhang and N. Chen</i> | 5185 |

About the Cover: The cover describes the progression of the 2013 Rim Fire from ignition to extinction, as seen by the operational Active Fire Application Related Product (left) and the Firelight Detection Algorithm (FILDA, right), both using the same input data from the Visible Infrared Imaging Radiometer Suite (VIIRS) aboard the Suomi-NPP. The white arrow highlights the first nocturnal detection by VIIRS using FILDA at 2:43 A.M. PDT on 18 August 2013, 11 hours after ignition. For more information, please see “Improving Nocturnal Fire Detection With the VIIRS Day–Night Band,” by Polivka *et al.*, which begins on page 5503.